ChemComm

FEATURE ARTICLE

View Article Online
View Journal | View Issue

Cite this: *Chem. Commun.*, 2022, **58**, 12642

Progress in the past five years of small organic molecule dyes for tumor microenvironment imaging†

Sha Li,[ab] Fangjun Huo[c] and Caixia Yin*[ab]

The tumor microenvironment (TME) is the survival environment for tumor cell proliferation and metastasis in deep tissues. Prognostic factors, such as growth, invasion and metastasis of malignant tumors, are closely related to changes in physiological parameters, including hypoxia, enzymes, low extracellular pH, and reduction conditions. Therefore, it is of great clinical significance to study tumor microenvironment markers to evaluate tumor progression and predict therapeutic effects. Organic fluorescent dyes are popular because of their small size, easy modification, adjustable luminescence and simple elucidation of their mechanism, and are widely used in tumor diagnosis and treatment. This paper reviews recent progress in fluorescent probes based on small organic molecules for imaging TME markers. Firstly, the design mechanism of a fluorescent probe is discussed, and then the application of pH, hypoxia, and reactive oxygen species, and a reduction-condition-responsive fluorescent probe in tumor imaging is discussed in detail. Finally, the prospects for the application of small-molecule fluorescent probes for imaging a tumor microenvironment *in vivo* are explored, but the potential application of small-molecule fluorescent probes in the early diagnosis of cancer as well as in the clinical laboratory for differentiating cancers, and further use in image-guided tumor surgery still face great challenges.

Received 8th September 2022,
Accepted 19th October 2022

DOI: 10.1039/d2cc04975a

rsc.li/chemcomm

The tumor microenvironment (TME) contains tumor cells, abundant mesenchymal cells and a variety of bioactive molecules, providing a heterogeneous and complex environment for tumor cell proliferation and metastasis. Prognostic factors such as growth, invasion and metastasis of malignant tumors are closely related to changes in physiological parameters, including hypoxia,[1–4] enzymes, low extracellular pH, and reduction conditions.[4–6] For example, hypoxia is thought to be a common feature of the TME, which is associated with changes in cell behavior, extracellular matrix remodeling, and increased metastatic behavior. Hypoxia is a feature of the TME caused by insufficient hypoxia supply,[7–9] which is closely related to tumor occurrence, malignant progression, tumor metastasis and treatment resistance.[10,11] In addition to a wide range of intracellular molecular and metabolic adaptations, hypoxic tumor cells also communicate extensively with the TME, creating favorable conditions for their survival, growth, metastasis and diffusion, making tumor cells more invasive. Therefore, it is of great clinical significance to study the degree of tumor hypoxia in evaluating tumor progression and predicting therapeutic effects.[12,13] Biomarker detection is an important method for the detection of tumor tissue hypoxia with high selectivity and sensitivity.[14–16] Hypoxia is usually associated with the elevation of some reductive enzymes, such as nitrate reductase (NTR), pantetheinase, and β-galactosidase. Under hypoxia, related enzyme activities of tumor cells increase, making enzymes an important target for the accurate and efficient detection of hypoxia in tumor cells or solid tumors.[10,17] Therefore, the sensitive and rapid detection of related enzyme activities can be used to evaluate the hypoxia level of tumors.[18] In addition, as an important physiological factor, intracellular pH is closely related to enzyme activity, cell apoptosis, cell proliferation and many other biological processes.[19–23] Reduced extracellular pH is also considered a marker of cancer, because lactic acid produced by high aerobic glycolysis[3] can induce apoptosis, promote angiogenesis by affecting the concentration of vascular endothelial growth factor, and affect enzyme activity by enhancing invasion ability.[24–26]

Redox conditions are central to human biochemical processes. For example, biomolecules containing sulfhydryl groups, such as cysteine (Cys) and glutathione (GSH), are important antioxidants in animal cells. Studies have shown that the concentration of reduced glutathione is much higher in tumor tissues than in healthy tissues. In addition, reactive oxygen species (ROS), such as hydrogen peroxide (H_2O_2), hypochlorous acid (HClO) and other

[a] *Department of Chemistry, Xinzhou Teachers University, Xinzhou 034000, China*
[b] *Key Laboratory of Chemical Biology and Molecular Engineering of Ministry of Education, Institute of Molecular Science, Shanxi University, Taiyuan 030006, China. E-mail: yincx@sxu.edu.cn*
[c] *Research Institute of Applied Chemistry, Shanxi University, Taiyuan 030006, China*

† Electronic Supplementary Information (ESI) available: Experimental section, synthesis, supplementary figures and imaging results. See DOI: https://doi.org/10.1039/d2cc04975a

bioactive molecules interact to provide essential nutrients and survival conditions for abnormal proliferation and metabolic patterns of tumor cells. There is growing evidence that cancer cells generally show increased endogenous ROS stress compared to normal cells.[27–29] Therefore, tumor-associated redox species are also alternative targets for designing response probes. Abnormal production and interaction of ROS are common phenomena in most TMEs.[6,30] Tracking ROS in a TME will provide strong evidence for elucidating tumorigenesis and further tumor therapy.

Therefore, it is of great significance to design and develop detection techniques that target TME parameters and clarify their relationships. As a powerful detection technology, a fluorescent probe has unique advantages in the detection of substances *in vivo*, such as high sensitivity, good temporal and spatial resolution, and non-invasive operation.[31–34] Due to the excellent performance of fluorescent probes, more and more TME-specific fluorescent probes have been developed.[35–37] Unfortunately, most probes emit in the spectral range of UV-vis light (below 650 nm), which is greatly disturbed by background self-fluorescence and low tissue penetration depth.[48–50] For quantitative detection of TMEs, near-infrared (NIR) fluorescent probes are more advantageous, with large penetration depth and little damage to biological samples.[51–54] Therefore, it is still a great challenge to develop a sensitive probe with an NIR fluorescence emission window that can accurately measure TME parameters. This paper reviews recent achievements in the design of small-molecule fluorescent probes for TME markers. Based on the first report of the detection of TME markers, an NIR fluorescent probe was developed to reduce photon scatter and tissue autofluorescence, and enhance deep tissue penetration in response to single and multi-site TME markers, resulting in real-time, high-resolution, cellular and *in vivo*-level imaging of the TME, with emphasis on building tumor model targeting applications.

In order to target a single tumor-related microenvironmental biomarker, the ideal "turn-on"-type responsive fluorescent probe should hardly emit in the blood or a normal tissue microenvironment, while being highly luminescent in the tumor microenvironment. A recognition mechanism needs to be designed that can activate small-molecule fluorescent probes, including fluorescence resonance energy transfer (FRET), photo-induced electron transfer (PET), intramolecular charge transfer (ICT) and other principles. In addition, the ratio-type responsive optical fluorescent probe will also be discussed below. In the following, the application of reducing conditions, enzymes, pH and hypoxia-responsive fluorescent probes in tumor fluorescence imaging will be discussed in detail.

Single stimuli-responsive fluorescent probes

Redox-sensitive fluorescent probes

Redox conditions are the center of various human biochemical processes. For example, biomolecules containing sulfhydryl groups, such as cysteine (Cys) and glutathione (GSH), are important antioxidants in animal cells. Studies have shown that the concentration of reduced glutathione in tumor tissues is much higher than that in healthy tissues. In addition, reactive oxygen species (ROS), such as hydrogen peroxide (H_2O_2) and hypochlorous acid (HClO), play an irreplaceable role in the signal transduction, metabolism and energy production of various tumors. Therefore, tumor-related redox species are also alternative targets for designing reaction probes.

In order to further explore whether GSH can be used as a biological indicator to identify tumor lesions at the cellular level, it is important to detect and accurately quantify GSH with high selectivity under pathological conditions. Recently, Yu's team designed a two-photon fluorescent probe Cou-Br based on coumarin derivatives (Fig. 1(A)).[55] The brominated functional component acts as a fluorescence modulator to identify intracellular GSH. Due to the heavy atom effect of the bromine atom, the probe is originally non-fluorescent. In the presence of glutathione, the brominated group can be replaced by the sulfhydryl group (–SH) in glutathione through a strong nucleophilic reaction, accompanied by strong fluorescence emission. The fluorescence signal is positively correlated with the level of glutathione in the cell, and the probe can image glutathione in various cell lines in real time. Carbon disulfide (CS_2) significantly increases the level of ROS (such as H_2O_2) in living cells, which in turn leads to cell apoptosis through a variety of signaling pathways.[56,57] Since biological thiols have the function of scavenging reactive oxygen species, exogenous ROS stimuli can directly change the level of GSH in cells, and the probe Cou-Br can detect this change. In this experiment, two groups of FaDu cells were incubated with cysteine and CS_2, respectively. A third group processed cysteine and CS_2 in order. As shown in Fig. 1(D), after adding exogenous Cys, the level of intracellular GSH increased, and the level of H_2O_2 decreased significantly. When incubated with CS_2 alone, the cells showed almost no fluorescence in Ch1, but showed a high ratio signal in the red channel (Ch_3/Ch_2). This phenomenon can be explained by the fact that after a certain amount of exogenous CS_2 is added, the intracellular GSH is significantly reduced, and

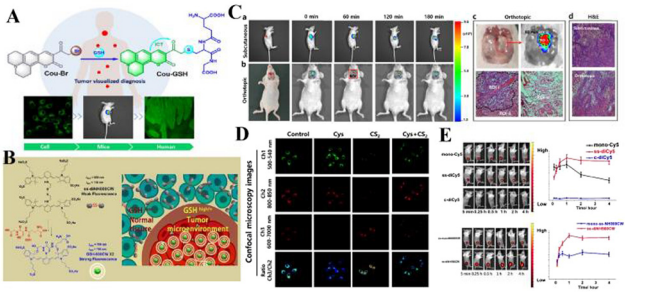

Fig. 1 (A) Molecular structure of Cou-Br and Its proposed response mechanism toward GSH. (B) Glutathione-responsive disassembly of disulfide dicyanine for tumor imaging. (C) Time-dependent fluorescence images in subcutaneous and orthotopic laryngeal carcinoma mice models. (D) Detection of GSH fluctuation in living FaDu cells with Cou-Br. (E) *In vivo* bioimaging picture and changes influorescent signals strength for tumor-bearing mice at various times. (A) and (C) Reproduced from ref. 55 with permission of the American Chemical Society, copyright 2020. (B), (D) and (E) Reproduced from ref. 58 with permission of Ivyspring, copyright 2020.

the H_2O_2 level is significantly increased. These results indicate that exogenous CS_2 can induce a burst of H_2O_2 in cells, causing severe oxidative damage, accompanied by a decrease in GSH concentration and induced cell apoptosis. Adding Cys (converted into GSH in the cell) can eliminate ROS, maintain the redox homeostasis of the cell, and reduce the rate of apoptosis. Fig. 1(C) shows *in situ* and real-time imaging of glutathione in a mouse model of laryngeal cancer. The increase in fluorescence intensity from 0 to 60 min indicates that the probe accumulates in the subcutaneous solid tumor over time. Similar results were observed in the *in situ* model. In the magnified image of the tumor *in situ* 60 minutes later, the fluorescence signal at the tumor lesion is significantly stronger than that in the surrounding tissue, indicating that the level of GSH in the tumor tissue is higher. The application of the probe in a tumor-bearing mouse model verified its *in vivo* bioimaging and tumor recognition capabilities. In summary, the proposed probe Cou-Br may become a powerful chemical tool for clinical cancer surgical navigation.

In order to more effectively identify tumor boundaries and distinguish tumor cells from healthy tissues during tumor surgery, Mo's team synthesized two near-infrared (NIR) fluorescent probes that are sensitive to glutathione (GSH), disulfide bond dicyanide amine dyes (ss-diCy5 and ss-diNH800CW) (Fig. 1(B)).[58] Since the synthesized dyes are quenched under normal physiological conditions, once they reach the tumor site, these dyes can emit a strong fluorescent signal, mainly because the disulfide bond breaks in the tumor microenvironment with high GSH concentration. Then the spectral properties of disulfide dicyanine dyes in the presence of glutathione were studied. After GSH treatment, the absorption band at 590 nm decreases, and the absorption band at 650 nm increases. The optical properties indicate that there is a serious aggregation phenomenon of dicyanide, which leads to fluorescence quenching, and the brightness of the fluorescence imaging probe is low. However, in the redox environment of the GSH solution, the fluorescence signal of the dithiocyanide dye increased by 27 times. Based on this, the fluorescence recovery performance of synthetic dyes was studied in tumor-bearing mice. Nearly 5 min after intratumoral injection of ss-diCy5 and mono-Cy5, the fluorescence signal was clearly visible; while there was almost no fluorescence after injection of c-diCy5. Fluorescence continued to increase after injection of ss-diCy5, reaching a maximum in 1 h and lasting for more than 3 h (Fig. 1(E)). NH800CW dye also shows the same trend. The fluorescence enhancement of ss-diNH800CW is more obvious. Interestingly, the fluorescence intensity of ss-diCy5 and ss-diNH800CW is higher than for the corresponding single dyes. Studies on cell uptake and tumor-bearing mice show that in cancer cells and tumor tissues, the disulfide bonds of dithiocyanate can be cleaved and produce a strong fluorescent signal. The results show that the dithiodicyandiamide dye can provide a promising platform for GSH-triggered tumor-specific fluorescence imaging.

Reactive oxygen species (ROS) are normal by-products of respiration and act as signal molecules at low concentrations. During oxidative stress, an antioxidant system in which the intracellular ROS concentration exceeds the capacity develops a series of pathologies in which ROS play a key role, including cancer, and neurodegenerative and cardiovascular diseases. After malignant transformation, abnormal cancer cell proliferation and metabolism and a complex tumor microenvironment will lead to very high levels of ROS. Fan's team developed a mitochondrial-specific orange/near-infrared emission fluorescent probe TTPB for the dual imaging of viscosity and H_2O_2 levels in two different channels.[59] TTPB is composed of a pyridine cation (the electron-acceptor part, a), phenylboronic acid unit, ethylene (a π-bridge), thiophene (a π-bridge and electron-donor group, D) and triphenylamine (D), showing a typical D–π–A molecular configuration, so it shows near-infrared fluorescence emission characteristics. Phenylboronic acid was selected as the dual sensor for the H_2O_2/viscosity of the H_2O_2 reaction unit. The probe shows an obvious response to viscosity at a wavelength of 666 nm, and a higher sensitivity to H_2O_2 at 586 nm. TTPB has good mitochondrial specificity and can separately detect the near-infrared channel viscosity of living cells and the orange channel H_2O_2 level. Based on significant results for live-cell imaging for malignant tumor model viscosity and H_2O_2 dual imaging, TTPB was finally applied to the simultaneous monitoring of H_2O_2 level and viscosity in biopsies. Normal tissues (heart, liver, spleen, lung, kidney, thymus) and tumor tissues were treated with TTPB for 30 min. Compared with the very weak fluorescence signal of normal tissue, tumor tissue shows an obvious significant increase in orange channel (H_2O_2) and near-infrared channel (viscosity) fluorescence, indicating that when the level of H_2O_2 in tumor tissue is increased, the viscosity increases. The above results vividly illustrate that TTPB can penetrate into tissues in the malignant tumor model, and the viscosity and H_2O_2 content have been double-imaged.

Liu's team reported that an NH-MT probe can selectively react with overexpressed H_2O_2 between tumor cells and emit strong fluorescence.[60] The results show that NH-MT not only responds to H_2O_2 in cells and zebrafish, but also has a good screening ability for tumor cells. In addition, this study also verified the targeting ability of melatonin, providing a new design idea for the construction of fluorescent probes for cancer cell screening, and developing a potential early cancer diagnostic tool (Fig. 2).

Reactive oxygen species (ROS) and cellular oxidative stress have long been associated with malignant tumors. Unfortunately, the role of HClO in tumor biology is far less clear than other ROS. Peng's team reported that a BODIPY-based HClO probe (BClO) has an ultra-sensitive, fast response (within 1 second) and high selectivity.[61] The pyrrole group at the *meso* position has an "enhanced PET" effect on the BODIPY fluorophore. The probe BClO consists of the fluorophore of boron dipyrrole (BODIPY) and 2,4-dimethylpyrrole (2,4-dimethylpyrrole). It is easily synthesized by a Michael addition reaction between one acryloyl chloride molecule and three 2,4-dimethylpyrrole molecules (Fig. 3(A)). The detection limit is as low as 0.56 nM. The Michael addition reaction of acryloyl chloride and 2,4 dimethylpyrrole can easily synthesize BClO, and is the first application of basic HClO imaging in cancer cells, and elesclomol induces the time-dependent

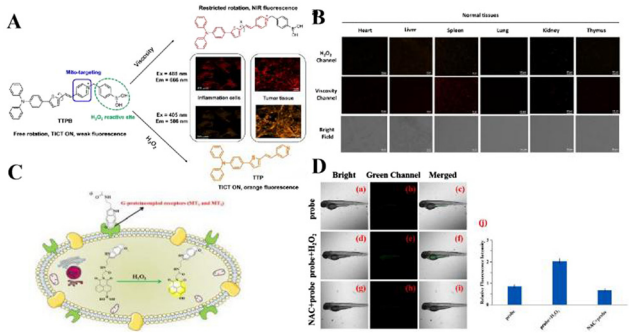

Fig. 2 (A) The structure and mechanism of TTPB for dual-response to mitochondrial viscosity and H_2O_2. (B) Fluorescence dual-images of TTPB in living normal tissues and tumors. Reproduced from ref. 59 with permission of Wiley, copyright 2021. (C) Molecular structure of NH-MT and its proposed response mechanism toward H_2O_2. (D) Fluorescence imaging of H_2O_2 in zebrafish. Reproduced from ref. 60 with permission of Elsevier B.V., copyright 2022.

production of HClO in MCF-7 cells (Fig. 3(B)). Therefore, BClO provides a promising chemical tool for the study of HClO in tumor biology and a molecular understanding of the mechanism of action of elesclomol.

The above-mentioned probes have been used to explore the relationship between cancer cells and HClO. However, few probes are used for the visual imaging of HClO during the growth of solid tumors *in vivo*. Therefore, it has become an urgent task to construct a fluorescent probe with high sensitivity, specificity, and rapid detection of HClO in tumors. Li's team constructed an HClO-specific trigger fluorescence release platform based on resorcinol dyes for the rapid detection of HClO *in vivo* and *in vitro*.[62] This is the first report of a probe molecule that specifically detects HClO based on N-protected resorcinol. Li *et al.* tried to use REC10-6 for the fluorescence imaging of HClO in solid tumors. The probe (REClO-1-REClO-6) has no inherent fluorescence. In the presence of HClO, the amide bond is specifically oxidized and broken, thereby restoring the red

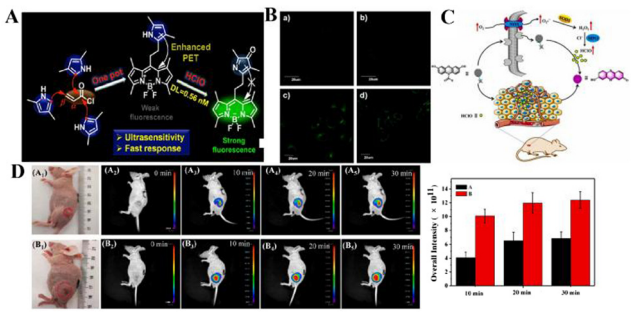

Fig. 3 (A) Construction principle and response mechanism of BClO. (B) Fluorescence images of normal and cancer cells after incubation with BClO for 20 min. Reproduced from ref. 61 with permission of the American Chemical Society, copyright 2014. (C) Molecular structure of RECl0-6 and its proposed response mechanism toward HClO. (D) Fluorescence imaging of mice with different tumors sizes using RECl0-6. Real-time imaging of subcutaneous tumors models in mice after intratumoral injection of the probe RECl0-6. Reproduced from ref. 62 with permission of Elsevier B.V, copyright 2021.

fluorescence of the resorcinol dye with a broad π-conjugated structure (Fig. 3(C)). Because of the rapid reaction of HClO (<50 s), it has high selectivity and sensitivity. The probe REC10-6 has been successfully used for HClO imaging in cells, zebrafish, arthritis mouse models and solid tumors. As shown in Fig. 3(D), two tumor models with significant differences in volume were established under the mouse epidermis. REC10-6 was injected into the tumor site *in situ*, and fluorescence images were taken at different time points. 10 min after the probe was injected, there was an obvious fluorescence signal at the tumor site. Within 20 min, the intensity of the fluorescence signal gradually increased with time, and the intensity of the fluorescence signal was also found to be proportional to the tumor volume. This is because the degree of tumor inflammation is different at different stages. Therefore, the high expression of HOCl in solid tumors may be the result of the high level of inflammation in the tumor site. These results indicate that REC10-6 can be used as an analysis tool for the visual monitoring of HClO in tumors.

Disrupting redox homeostasis in TMEs, such as excessive H_2O_2 and GSH, has been proved to be an effective tumor treatment strategy. Within a TME, ROS regulates redox homeostasis and promotes oxidative stress. With the further study of TMEs, more and more roles of redox in TMEs have been found. The synergistic effect of different types of redox in different cells or organelles is considered to be an important event affecting tumor proliferation, metastasis and drug resistance. However, due to the lack of available research tools, most of their detailed mechanisms have not been revealed. In the future, it will be necessary to discover further ROS and fluorophore recognition mechanisms with excellent performance, to explore new targeting mechanisms and imaging strategies for different cell types in TMEs.

Enzyme-sensitive NIR fluorescent probes

In monitoring physiological and pathological processes at the molecular and cellular level, particularly worthy of attention is the application of NIR emission (650–900 nm) fluorescent molecules in living systems, because they can significantly avoid autofluorescence, reduce photon scattering, and improve the penetration of deep tissues. Fluorescent probes have the ability to selectively display tumor sites and metastases. Enzyme-active near-infrared optical probes have the characteristics of fast response time and good pharmacokinetics. They have shown great potential in tumor diagnosis and a high signal-to-noise ratio in image-guided intraoperative surgery. In recent years, significant progress has been made in the development of tumor overexpression enzyme fluorescent probes, which undoubtedly contribute to the early diagnosis and treatment of cancer. Related genes involved in tumorigenesis and development regulate the overexpression of certain enzymes. The latest advances in the design strategies and biomedical applications of NIR fluorescent probes for several enzyme activities closely related to the tumor microenvironment are described below.

NQO1 plays a protective role in the cellular oxidative stress response, but it is abnormally highly expressed in various solid cancers. Therefore it is considered a cancer biomarker. In order

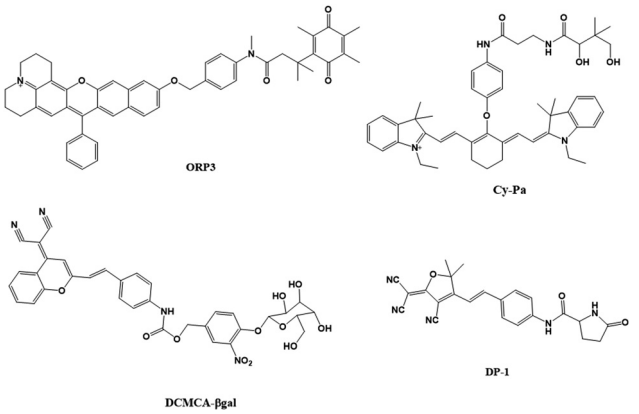

Fig. 4 List of enzyme-active near-infrared fluorescence probes.

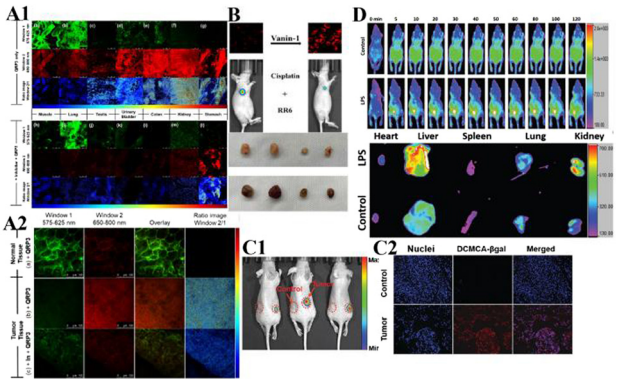

Fig. 5 (A1) CLSM fluorescence images of QRP3 in different mouse organ tissues: (a)–(g) incubated with QRP3 and (h)–(l) preincubated with dicoumarol as an inhibitor. (A2) CLSM fluorescence images of the mouse tissue: (a) normal and tumor (b) and (c) tissues incubated with QRP3 and (c) preincubated with dicoumarol. (B) Cy-Pa on effects of synergistic therapy with RR6 and cisplatin in HepG2/DDP tumor-bearing mice. Reproduced from ref. 64 with permission from the American Chemical Society, Copyright 2021. (C1) Fluorescence imaging of DCMCA-βgal in ovarian tumors. (C2) Fluorescence images of the dissected tumor tissues. (D) Fluorescence images of DP-1 in normal/inflammation mice. Reproduced from ref. 65 with permission of the Royal Society of Chemistry, copyright 2021.

to develop a practical ratiometric NQO1 probe, Dai's team recently developed an ether-linked, hydrolytically stable probe QRP3 that was applied to the ratio imaging of NQO1 in cells and tissues (Fig. 4).[63] Given that QRP3 can perform the effective ratio imaging of cellular NQO1 activity, we then applied the probe to compare the NQO1 levels in different mouse organs and tissues. Seven different organs and tissues were prepared and the I_{red}/I_{green} value of each organ tissue were compared: stomach (28), kidney (11), colon (4.9), testis (3.9), bladder (2.8), lung (0.6), and muscle (0.5). This trend represents the relative activity level of NQO1 in organs and tissues, which was determined for the first time by fluorescence imaging (Fig. 5(A)). Next came the imaging of NQO1 in tumor tissue. A high expression of NQO1 is associated with cancer; its level is abnormally elevated in solid tumors, including breast, pancreatic, gastric, lung, and ovarian cancers. Therefore, NQO1 is a potential cancer biomarker. A549 cancer cells were injected subcutaneously into the right thigh of BALB/c mice to generate tumors. Tumor tissue sections and normal tissue sections of xenotransplanted mice were prepared from the other thigh. Compared with normal tissues, the I_{red}/I_{green} value of the tumor tissues was significantly higher at 14.6 (Fig. 5). When the tumor tissue was pre-incubated with diflavin, the I_{red}/I_{green} value decreased, which also supports the theory that the change in the ratio is due to enzyme activity on the probe. The significant tumor/normal discrimination factor indicates the potential application of QRP3 in the clinical laboratory identification of cancer and imaging-guided tumor surgery.

Pantetheinase (also known as vanin-1) is highly expressed in the liver, kidneys and intestines, and is closely related to many diseases, and vanin-1 is involved in the synthesis of glutathione (GSH). GSH is highly expressed in tumor cells and plays an important role in the resistance of tumor cells to cisplatin. Therefore, Huang's team reported that Cy-Pa, an NIR fluorescent probe emitting at 780 nm, can be used to image vanin-1 in cells and *in vivo*, which can qualitatively and quantitatively detect HepG2 and HepG2/DDP cells in tumor-bearing mice, or fluctuations in the concentration of vanin-1 in tumor tissues.[64] As shown in the experiment shown in Fig. 5(B), the addition of RR6 in the course of tumor chemotherapy can inhibit the activity of vanin-1, thereby reducing the efficacy of the chemotherapy drug cisplatin, resulting in a decline in its therapeutic effect on tumors. This protective effect on cells may be due to the increased storage of GSH when vanin-1 activity is inhibited, thereby weakening the killing effect of chemotherapy on tumor cells. The Cy-Pa probe developed in this research can accurately detect changes in the activity of vanin-1 at the cellular level and *in vivo* in real time, which is helpful for the treatment of tumors.

Because β-galactosidase (β-gal) is overexpressed in primary ovarian cancer, it is considered to be an important ovarian cancer biomarker. Shi's team recently reported a sensitive β-gal activation probe (DCMCA-βgal) for the NIR imaging of ovarian tumors.[65] After adding β-gal to DCMCA-βgal, due to the generation of DCM-NH2, a significant fluorescence enhancement was produced at about 680 nm. DCMCA-βgal has the advantages of high sensitivity, good light stability in dynamic life systems, and a large spectral shift. It can well visualize β-gal activity in SKOV3 human ovarian cancer cells and can image ovarian cancer mouse models in real time. Shi *et al.* subcutaneously inoculated the left and right sides of the mouse with control 293T cells and SKOV3 cells to construct a mouse model of ovarian cancer. As shown in Fig. 5(C), 10 min after DCMCA-βgal was injected into the tumor, a significant near-infrared fluorescence signal was detected on the right flanks which gradually increased; however, even 1 h after injection, there was no fluorescence signal on the left side. In addition, fluorescence imaging of tumor tissues showed that compared with the control group, the NIR fluorescence signal of ovarian tumors increased significantly. This result further confirms that DCMCA-βgal can be used to visualize and track β-gal activity in ovarian tumors, and thus provides a convenient tool for imaging ovarian tumors, which provides a huge preclinical potential for the early diagnosis and treatment of ovarian cancer.

Pyroglutamate aminopeptidase-1 (PGP-1) is an important enzyme that plays an indispensable role in the inflammation process. For the first time, Qinet's team designed and synthesized a long emission ratio fluorescence sensor (DP-1) that can specifically detect PGP-1 *in vivo* and *in vitro*.[66] After the probe reacts with PGP-1, it is hydrolyzed by the PGP-1 amide bond, and the fluorescence emission wavelength changes from 564 nm to 616 nm. This probe has been effectively used for imaging PGP-1 in HepG2 and RAW264.7 cells under the action of inflammation inducers. This also proves that under the action of the inhibitor, the expression of the enzyme is significantly reduced. In order to further prove that the upregulation of PGP-1 is related to the inflammation process, Qin *et al.* injected the probe into inflammation model mice pre-cultured with LPS for imaging. Fig. 5(D) shows the abdominal images of the above two groups of mice at 0–90 min. With increasing time, the fluorescence intensity of the abdomen of the mice in the LPS group gradually increased to the maximum value, then slowly decreased, and the fluorescence intensity was significantly stronger than that of the control group injected only with the probe. The imaging results of inflammation model mice showed that the enzyme content did increase after drug induction. In addition, by imaging the main organs of inflamed mice, it was found that fluorescence mainly appears in the liver, kidney and lung tissues. The fluorescence intensity of the liver and kidney is much greater than that of lung tissue. According to the results of imaging experiments in inflammation model mice, DP-1 can effectively monitor the expression of enzymes in inflammation mice in real time. Next came real-time monitoring and imaging of mouse tumor cell PGP-1 activity. Experimental phenomena show that the expression of this enzyme in tumor mice is much higher than that in normal mice, suggesting that the expression level of PGP-1 in living organisms is closely related to the occurrence of certain diseases, such as tumors. The imaging experiments of tumor model mice further confirmed that PGP-1 is closely related to the occurrence of tumors, which provides detection potential for research into PGP-1 related diseases (such as tumors) in the biomedical field.

Although there have been a lot of developments in the early diagnosis and treatment of tumors with enzyme-reactive fluorescent probes in recent years, there are still many problems to be solved. For example, fluorophores have deeper tissue penetrability and a higher signal to noise ratio, and will be widely used in diagnosis and medical fields; most fluorescent probes can simply distinguish between normal cells and cancer cells, but cannot identify specific tumor cell types. Therefore, a multi-target, enzyme-activated fluorescent probe based on a cascade reaction will provide a strategy for identifying specific cancer cells and tumors *in vivo*.

pH-sensitive NIR fluorescent probes

Due to the metabolic accumulation of lactic acid, the acidic tumor tissue microenvironment (<6.8) is considered to be a universal feature of the tumor microenvironment, which can distinguish tumors from normal tissues. The study of pH probes can provide an operable system for tumor treatment and imaging. pH imbalance is considered to be a sign of cancer. The close relationship between cell function and extracellular pH means that accurate and real-time measurement of the dynamic changes in extracellular pH can be used not only for the study of physiological and pathological processes but also for cancer and other diseases. The diagnosis provides important information.

As an important physiological factor, intracellular pH is closely related to many biological processes such as enzyme activity, cell apoptosis, and cell proliferation.[38–44] The specific pH value of the organelle is a necessary condition for the intracellular pH value. An acidic environment is a necessary condition for lysosomes to maintain normal physiological functions. Abnormal fluctuations in lysosomal pH can lead to diseases such as cancer and Alzheimer's disease.[45–48] Based on this, Yin's team proposed a new type of ratiometric fluorescent probe (SN-Lyso) and dual mechanism (ICT-FRET) to detect lysosomal pH fluctuations (Fig. 6(A)).[67] SN-Lyso responds with red and green emission to acid and alkali pH changes, respectively. At the same time, SN-Lyso has been successfully applied to fluorescence imaging of living cells. Studies have found that autophagy cells can cause a decrease in lysosomal pH. Chloroquine, as a lysosomal prokinetic agent, can inhibit autophagy and protein degradation by increasing lysosomal pH.[32] It can be seen from Fig. 7(A) that the green fluorescence of cells treated with chloroquine increased, and the red fluorescence decreased, indicating that the pH of the lysosome increased. Then, Yin *et al.* used SN-Lyso to monitor pH to evaluate the tumor microenvironment and normal microenvironment of the mouse model. SN-Lyso was injected into the tumor site and right lower limb of female nude mice. In the red channel, there was a clear fluorescence signal at the tumor site of the mouse, while a very weak fluorescence signal appeared at the normal site (Fig. 7(B)). These results indicate that in the mouse model, the tumor microenvironment is more acidic than the normal microenvironment. In this article, SN-Lyso can provide an effective method for studying the pathological mechanism of lysosomes and visualizing the treatment of tumor sites.

Existing pH-responsive fluorescent probes are hindered by rapid clearance or high liver background emission, so there is still a need to design water-soluble, long-cycle, pH-responsive nanoprobes with high tumor–liver contrast agents. Based on

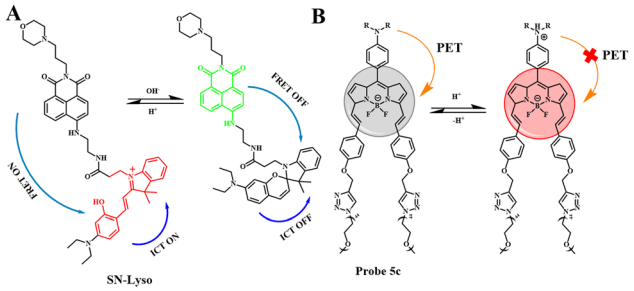

Fig. 6 List of reaction mechanisms for PH-sensitive NIR fluorescent probes.

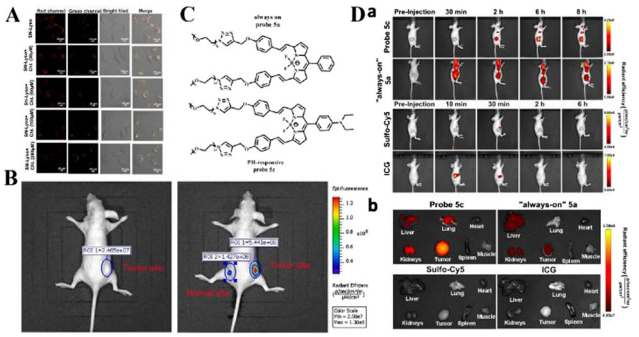

Fig. 7 (A) PH imaging in lysosomes of HeLa cells stimulated with 0, 30, 60, 100 and 200 μM chloroquine. (B) *In vivo* fluorescence imaging of SN-Lyso (10 μM) for the tumor site and the normal site in HeLa-tumor-bearing nude mice. Reproduced from ref. 67 with permission of Elsevier B.V, copyright 2021. (C) Structural formulae of probe 5a and probe 5c. (D) Probe 5c activates in the low-pH tumor microenvironment. (a) Time-dependent *in vivo* fluorescence images of mice bearing subcutaneous tumors. (b) Representative fluorescence images of harvested tumors and organs from tumor-bearing mice sacrificed at 6 h (sulfo-Cy5 or ICG) post injection. Reproduced from ref.68 with permission from the American Chemical Society, Copyright 2016.

this, Siegwart *et al.* used the PET effect to successfully develop a series of water-soluble, pH-adjustable NIR BODIPY fluorescent probes (Fig. 6(B)).[68] pH-responsive probe 5c can achieve NIR (>650 nm) emission, can be localized in cancer cells in the body, and is activated by acidic pH, resulting in high signal contrast between mice with lung cancer and cervical cancer and normal mice and high signal contraction of liver tumors after intravenous injection of breast cancer cells. This new type of small-molecule probe is a promising step in detecting different cancer cells without attaching tumor-targeting groups. Based on the results of cancer cell imaging, Siegwart *et al.* chose probe 5c as a promising probe for *in vivo* tumor imaging. Probe 5c can locate tumors in mice and "open" after intravenous injection. Next, the ability of probe 5c to activate in tumors after intravenous injection was evaluated. Mice carrying MDA-MB-231 subcutaneous tumors can activate probe 5c or probe 5a that is always on by intravenous injection of pH, and observe strong and continuous radiation (Fig. 7(C)). To further prove the improved PK, intravenous injection of water-soluble sulfo-Cy5 and ICG dye were compared. Only 15 min later, sulfo-Cy5 and ICG staining can be seen in the liver and kidneys due to the rapid clearance by the kidneys (Fig. 7(D)), and it was almost completely cleared within 2 h. These results indicate that probe 5c has a higher accumulation and activation ability in tumors, and because pegylation prolongs blood circulation time, the clearance rate of probe 5c in tumor-bearing mice is much slower than that of sulfo-Cy5 or ICG. This report introduces a general strategy to directly synthesize soluble probes with a wide range of potential uses, including fluorescence-based image-guided surgery, cancer diagnosis, and therapeutic nanomedicine.

For cancer cells and tissues, the accumulation of pH-activated fluorescent probes directed by specific tumor-targeting ligands shows attractive potential in tumor-reversible and high signal-to-noise imaging. However, there is little tracking of pH *in vivo*, which is not conducive to revealing the relationship between mitochondrial pH abnormalities and diseases. In the future, NIR and TP probes should be developed for the visualization of mitochondrial pH in disease models.

Hypoxia-sensitive NIR fluorescent probes

Hypoxia is defined as a decrease in the level of oxygen in the tissue. In the case of hypoxia, tumor cells will be stimulated to secrete vascular growth factors, promote the formation of abnormal blood vessels, and then the tumor will metastasize and worsen.[37] In addition, the hypoxic microenvironment has a screening effect on tumor cells, increasing the malignancy of tumors, and then making tumor cells resistant to chemotherapy or radiotherapy. Therefore, it is necessary to develop effective methods to detect tumor cells and hypoxic conditions in the body. Hypoxia-sensitive fluorescent probes can monitor the hypoxia state of tumor cells by detecting endogenous upregulated reductase, while NIR fluorescent probes have the advantages of good tissue penetration and low biological and auto-fluorescence damage, and can be used for hypoxic tumor imaging.

Li *et al.* developed two NIR hypoxia-sensitive probes (AXNO2 and AXNN, shown in Fig. 8(A)), on the basis of there being no current reports of fluorescence probes that can detect hypoxia by combining hypoxia-regulating enzymes.[69] AXPI with an amino group was synthesized by two-step decomposition of IR-780, introducing hypoxically activated *p*-nitrobenzene or azo fractions as sensing units. The reaction of both probes with hypoxic upregulation enzymes results in the cleavage or reduction of specific enzymes, resulting in the release of a red fluorophore (λ_{em} = 706 nm). The combined use of the two probes can successfully differentiate 4T1 and HepG2 cell lines through fluorescence signals. In addition, probes AXNO2 and AXNN were injected into tumor-bearing mice for hypoxic tumor imaging to monitor the changes in fluorescence intensity within the tumor. As shown in Fig. 9(A), a clear fluorescence signal is obtained from the tumor, which is clearly different

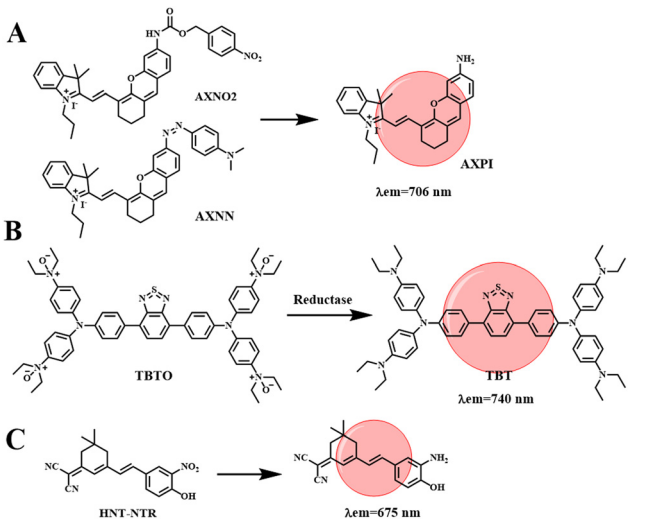

Fig. 8 List of reaction processes for hypoxia-sensitive NIR fluorescent probes.

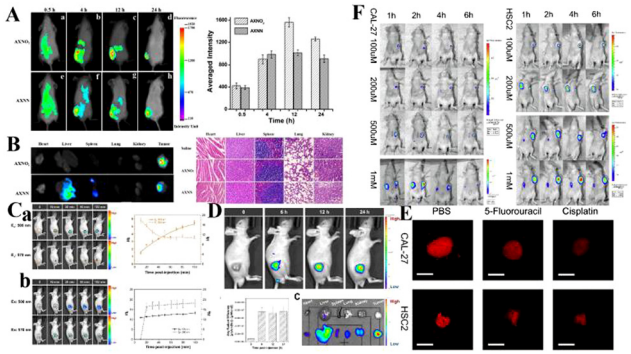

Fig. 9 (A) Time-dependent *in vivo* fluorescence imaging of mice after tail-vein injection of AXNO2 and AXNN. (B) Fluorescence images of major organs 24 h after injection and H&E staining images of the major organs. Reproduced from ref. 69 with permission from the American Chemical Society, Copyright 2018. (C) NIR fluorescence imaging of mice before and after intratumoral injection of (a) TBTO and (b) TBT before and after *in vivo* hypoxia activation. (D) Fluorescence imaging of TBTO in tumor-bearing mice *via* tail intravenous injection. (E) HNT-NTR imaged the hypoxia in tumor spheres which were treated with different chemotherapeutic drugs. (F) *In vivo* imaging of tumor-bearing mouse after injection of HNT-NTR. The mouse was implanted with Cal-27 and HSC2 cells. Reproduced from ref. 70 with permission from Elsevier B.V, Copyright 2021.

from the surrounding tissues. In order to determine that the fluorescent signal came from the probe accumulated in the tumor area, mice were sacrificed 24 h after injection, and the major organs (heart, liver, spleen, lung, kidney, and tumor) were captured (Fig. 9(B)). The results were consistent with *in vivo* observations, as specific reduction was only found in the tumor region. This research can improve the diagnostic sensitivity for malignant tumors, which is conducive to the early diagnosis, treatment and prognostic evaluation of cancer.

Constructing probes that respond to a tumor microenvironment with multiple imaging modes, especially hypoxia imaging for solid tumors, is an attractive but challenging task. Tang *et al.* designed an NIR hypoxic activation probe TBTO for *in vivo* imaging. TBTO (λ_{em} = 600 nm) can be bioreduced in a low-oxygen microenvironment to form the compound TBT (λ_{em} = 740 nm) with characteristics of NIR-aggregation-induced emission and strong intramolecular charge transfer (Fig. 8(B)).[70] The typical D–A–D structure of BT leads to a strong TICT effect, which causes the fluorescence emission to redshift to the NIR region. It promotes the generation of a PA signal and endows the probe with excellent NIR fluorescence and photoacoustic dual-mode tumor imaging performance. We subsequently studied the NIR imaging of hypoxia activation in tumor-bearing mice encouraged by *in vitro* hypoxia. HeLa cells were implanted subcutaneously into mice to construct an allograft tumor. To monitor the TBTO–TBT transformation in real time, two mice were injected with TBTO (Fig. 9(C)-a) and TBT (Fig. 9(C)-b) by intratumoral injection. The fluorescence signal collected by the 500 nm excitation filter was gradually weakened in the mice injected with TBTO, while the fluorescence signal collected by the 570 nm excitation filter was gradually enhanced, indicating that the reduction reaction of TBTO occurred in the hypoxic tumor. On the other hand, mice injected with TBT, stimulated at 500 nm or 570 nm, showed nearly constant near-infrared fluorescence intensity for 100 min after injection, since TBT was inactivated in the tumor microenvironment. In addition, TBTO has good optical stability. Tang *et al.* tested the tumor-targeting specificity and persistence of TBTO by tail-vein injection. As shown in Fig. 9(D), a distinct NIR fluorescence signal is detected in the tumor and the intensity lasts for more than 24 h. Images from major organs and tumors *in vivo* further confirmed TBTO accumulation in tumors. This work suggests a promising approach for clinical imaging that exploits the specific microenvironment of the lesion area, which may be useful in tumor diagnosis, image-guided surgical interventions, and evaluation of therapeutic efficacy.

Nitroreductase (NTR) is overexpressed in hypoxic tumors, making it an effective target for detection of tumor hypoxia. Zhang *et al.* developed a new nitro-based fluorescent probe HNT-NTR,[71] which can recognize NTR by converting a nitro to an amino group. After activation of NTR, the fluorescence intensity is enhanced at 675 nm, which can be used to detect and visualize NTR in complex biological systems. With the addition of NTR, the contact between tumor cells in 3D tumor spheres is similar to that of solid tumors *in vivo*, which can simulate the situation of solid tumors *in vivo*, so hypoxia, or NTR formation, can be detected in 3D tumor spheres. As shown in Fig. 9(E), the fluorescence intensity of 3D tumor spheres treated with chemotherapy drugs (cisplatin or 5-fluorouracil) was much lower than that of the control group. Secondly, Zhang *et al.* designed an experiment to study the effect of HNT-NTR on the NTR level in mouse CAL-27 and HSC2 tumors (Fig. 9(F)), and the fluorescence intensity in the tumor region was significantly increased. The results showed that HNT-NTR could effectively reflect the hypoxia level *in vivo* and evaluate the formation, development and even metastasis of tumors. It has broad application prospects in the detection of hypoxia *in vivo*.

Although the emission wavelength of the probes used to detect mitochondrial hypoxia mostly reaches the NIR region, researchers have not yet fully explored the use of these probes to detect endogenous hypoxia in complex biological systems. In the future, researchers need to pay attention to the qualitative and quantitative detection of hypoxia in diseases and physiological abnormalities.

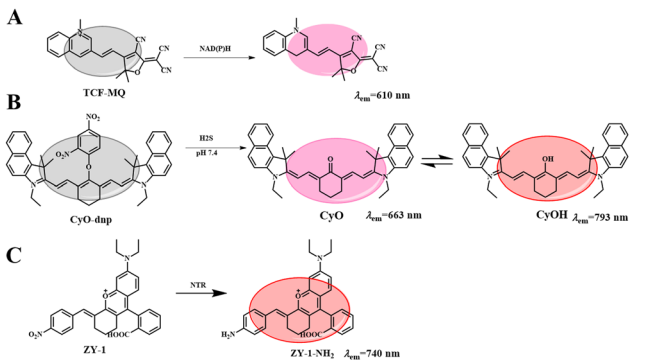

Fig. 10 List of reaction processes for multi-responsive of NIR fluorescent probes.

Multi-responsive NIR fluorescent probes

These probes usually respond to only one biological condition, but tumor progression is often the result of multiple biological factors. These physiological parameters in the tumor microenvironment are strongly correlated. Therefore, strategies that rely on multiple biomarkers have emerged in recent years. For example, Tang *et al.* reported the anticancer effects of reductive stress induced by three natural antioxidants (resveratrol, curcumin and celastrol).[72] First, an ultra-sensitive NIR fluorescent probe (TCF-MQ, Fig. 10(A)) was developed for the specific imaging of NAD(P)H. TCF-MQ reacted quickly to NAD(P)H with high sensitivity and the detection limit was 6 nM. The probe successfully imaged endogenous NAD(P)H in living cells and differentiated different levels of NAD(P)H in HepG2 cells under normoxic and hypoxic conditions. Taking into account the hypoxia in a solid tumor microenvironment, Tang *et al.* treated HepG2 cells with three natural antioxidants under hypoxic conditions. A high level of NAD(P)H was generated before cell death, and excessive NAD(P)H led to reductive stress. In order to further confirm the reductive stress of natural antioxidants on HepG2 cells under hypoxia, a similar experiment was conducted *in vivo*. Tumor-bearing mice were subcutaneously injected with resveratrol, curcumin and celastrol, and then injected with the TCF-MQ probe. The results were similar to those of the resveratrol treatment group, and the fluorescence intensity of the probe in the curcumin and celastrol treatment groups was enhanced. These results showed that NAD(P)H levels increased during the treatment of hepatocellular carcinoma cells with three natural antioxidants. Tumor volume measurement experiments showed that resveratrol significantly inhibited tumor growth in a dose-dependent and time-dependent manner (Fig. 11(A)-a). Curcumin and celastrol also inhibited tumor growth in mice (Fig. 11(A)-b, c), suggesting that reductive stress induced by the three natural antioxidants could inhibit tumor growth in liver cancer. The results revealed a new anticancer mechanism for resveratrol, curcumin and celastrol, providing a new field for the study of natural antioxidants.

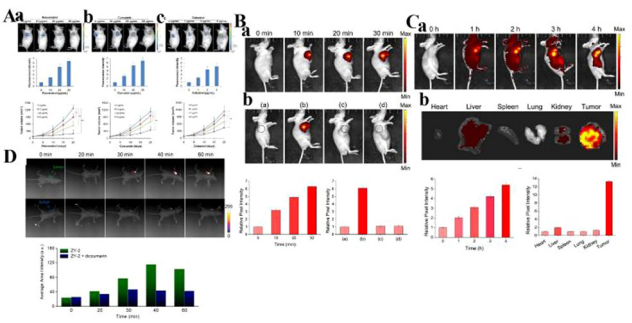

Fig. 11 (A) Detection of NAD(P)H levels induced by natural antioxidants (a: resveratrol; b: curcumin; c: celastrol) *in vivo*. Reproduced from ref. 72 with permission of the Royal Society of Chemistry, copyright 2019. (B) a. Fluorescence imaging of endogenous H_2S and H^+ in tumor mice through intratumoral injection of CyO-DNP over time. b. Fluorescence images of CyO-DNP in mice. (a) The normal mice and (b) the tumor mice were intratumorally injected with CyO-DNP, the tumor mice were injected with (c) $NaHCO_3$ or (d) AOAA and then injected with CyO-DNP. (C) (a) Fluorescence imaging of endogenous H_2S and H^+ in the tumor mice through tail intravenous injection of CyO-DNP. (b) Fluorescence imaging of *ex vivo* tumors and other major organs. Reproduced from ref. 69 with permission from the American Chemical Society, Copyright 2020. (D) *In vivo* fluorescence imaging of HeLa-tumor-bearing mice after intratumoral injection of ZY-2 at different time points. Reproduced from ref. 74 with permission of Elsevier B.V, copyright 2022.

In addition, endogenous H_2S is considered a cancer biomarker. Under physiological conditions, malignant tumors present an acidic microenvironment compared to normal tissues, and pH value is considered to be another important cancer marker. Therefore, finding a simple and sensitive method for detecting H_2S and H^+ tumor markers is very important for the accurate early diagnosis of tumors. Based on this, Li *et al.* synthesized a new NIR fluorescent probe (CyO-DNP, Fig. 10(B)) for the sequential detection of H_2S and H^+.[73] The probe selected a heptamethyl dye as fluorophore and a 2,4 dinitrobenzene (DNP) ether as the recognition group. In the presence of H_2S, CyO showed strong fluorescence at 663 nm. Then H^+ induced protonation of CyO to obtain CyOH (λ_{em} = 793 nm). CyO-DNP can continuously monitor endogenous H_2S and H^+ in cancer cells. Subsequently, a tumor-bearing mouse model was established by subcutaneous injection of 107HCT-116 cells into the armpit of nude mice. As shown in Fig. 11(B)-a, the fluorescence signal gradually increased over time, indicating that CyO-DNP responded to endogenous H_2S and H^+ in tumor-bearing mice. Meanwhile, as shown in Fig. 11(B)-b, normal mice showed no obvious fluorescence after subcutaneous injection of CyO-DNP. However, due to the high content of endogenous H_2S in the tumor and the acidic tumor microenvironment, the tumor site showed a strong near infrared fluorescence signal. These results suggest that CyO-DNP can accurately distinguish normal mice from tumor mice and is suitable for the early diagnosis of cancer. Then, CyO-DNP was injected into the tail vein of the tumor mice, as shown in Fig. 11(C)-a, and the fluorescence signal in the tumor area gradually increased over time. As shown in Fig. 11(C)-b, no fluorescence was found in kidney or liver after dissection. This is because normal organs such as liver and kidney overexpress H_2S, but their environment is neutral and cannot induce the final fluorescence emission of CyO-DNP. CyO-DNP is the first fluorescent probe to accurately diagnose cancer early by sequentially detecting H_2S and H^+. This strategy of sequential detection of two cancer markers may become an effective method for early cancer diagnosis in the future.

Nitrate reductase (NTR) is overexpressed in hypoxic cancer cells. Upregulation of the NTR level is considered a marker of hypoxia and also a tumor marker.[6] Therefore, it is urgent to monitor the expression of NTR in hypoxic tumors. Based on this, Shen *et al.* reported an NTR-activated NIR probe (ZY-1) with good selectivity and sensitivity (Fig. 10(C)).[74] After reaction with NTR, the probe showed a significant fluorescence turn-off response at 740 nm, achieving the accurate determination of NTR. The probe has been successfully used to evaluate the degree of hypoxia of cancer cells and to detect exogenous NTR. In order to further study the adaptability of ZY-2 *in vivo*, a HeLa-tumor-bearing mouse model was used. As shown in Fig. 11(D), moderate fluorescence was observed 20 min after injection,

indicating that ZY-2 reacted very quickly with NTR at the tumor site. The fluorescence increased gradually, reaching the maximum signal at 40 min; then the fluorescence intensity decreased with time, and disappeared 6 h after injection. Therefore, ZY-2 is conducive to elimination from the body. It is hoped that the probe will provide more opportunities to develop molecular tools for monitoring hypoxia in the body.

Conclusion and outlook

This paper reviews research progress into small-molecule fluorescent probes targeting tumor microenvironment markers over the past five years, and also verifies the targeting ability of tumor microenvironment markers, which provides a new design idea for the construction of fluorescent probes for cancer cell screening. Although progress has been made so far in the development of fluorescent probes based on organic small molecules in the cell microenvironment, there are still many unresolved challenges: (1) most probes exhibit short excitation (500 nm)/emission (600 nm) wavelengths, limiting their application *in vivo*. (2) Many probes display an open fluorescence signal, which may be interfered with by instrument parameters and dye concentration, reducing the accuracy of detection. (3) The poor water solubility of many probes limits their performance in biological systems. In addition, the small Stokes shift, high toxicity, low light stability and low signal-to-noise ratio should be improved. On this basis, an NIR fluorescence probe with more advantages, such as large penetration depth and less damage to biological samples, is considered to be a promising platform for designing response mechanisms to different stimuli, such as O_2, acidity, specific enzymes, and redox.

Conflicts of interest

There are no conflicts to declare.

Acknowledgements

We thank the National Natural Science Foundation of China (No. 22074084), One hundred people plan of Shanxi Province, Shanxi Province ''1331 project'' key innovation team construction plan cultivation team (2018-CT-1), 2018 Xiangyuan County Solid Waste Comprehensive Utilization Science and Technology Project (2018XYSDJS-05), Shanxi Province Foundation for Returness (2017-026), Shanxi Collaborative Innovation Center of High Value-added Utilization of Coal-related Wastes (2015-10-B3), the Shanxi Province Foundation for Selected (No. 2019), Innovative Talents of Higher Education Institutions of Shanxi, Scientific and Technological Innovation Programs of Higher Education Institutions in Shanxi (2019L0031), Key R&D Program of Shanxi Province (201903D421069), the Shanxi Province Science Foundation (No. 201901D111015), Key R&D and transformation plan of Qinghai Province (2020-GX-101) and Scientific Instrument Center of Shanxi University (201512).

Notes and references

1 B. A. Webb, M. Chimenti, M. P. Jacobson and D. L. Barber, *Nat. Rev. Cancer*, 2011, **11**, 671.
2 V. Estrella, T. A. Chen, M. Lloyd, J. Wojtkowiak, H. H. Cornnell, A. Ibrahim-Hashim, K. Bailey, Y. Balagurunathan, J. M. Rothberg, B. F. Sloane, J. Johnson, R. A. Gatenby and R. J. Gillies, *Cancer Res.*, 2013, **73**, 1524.
3 J. Rozhin, M. Sameni, G. Ziegler and B. F. Sloane, *Cancer Res.*, 1994, **54**, 6517.
4 D. Hanahan and R. A. Weinberg, *Cell*, 2011, **144**, 646.
5 K. Kessenbrock, V. Plaks and Z. Werb, *Cell*, 2010, **141**, 52.
6 M. A. Moses, D. Wiederschain, K. R. Loughlin, D. Zurakowski, C. C. Lamb and M. R. Freeman, *Cancer Res.*, 1998, **58**, 1395.
7 A. L. Harris, *Nat. Rev. Cancer*, 2002, **2**, 38.
8 F. He, X. Deng, B. Wen, Y. Liu, X. Sun, L. Xing, A. Minami, Y. Huang, Q. Chen, P. B. Zanzonico, C. C. Ling and G. C. Li, *Cancer Res.*, 2008, **68**, 8597.
9 M. P. Hay and W. R. Wilson, Targeting hypoxia in cancer therapy, *Nat. Rev. Cancer*, 2011, **11**, 393.
10 E. T. Shinohara and A. Maity, *Curr. Mol. Med.*, 2009, **9**, 1034.
11 K. J. Williams, M. R. Albertella, B. Fitzpatrick, P. M. Loadman, S. D. Shnyder, E. C. Chinje, B. A. Telfer, C. R. Dunk, P. A. Harris and I. J. Stratford, *Mol. Cancer Ther.*, 2009, **8**, 3266.
12 R. Kumari, D. Sunil, R. S. Ningthoujam and N. V. A. Kumar, *Chem. – Biol. Interact.*, 2019, **307**, 91.
13 H. Yang, Y. H. Geng, P. Wang, Y. T. Zhou, H. Yang, Y. F. Huo, H. Q. Zhang, Y. Li, H. Y. He, X. X. Tian and W. G. Fang, *Cancer Sci.*, 2019, **110**, 2456.
14 A. R. Padhani, K. A. Krohn, J. S. Lewis and M. Alber, *Eur. Radiol.*, 2007, **17**, 861.
15 W. R. Wilson and J. M. Brown, *Nat. Rev. Cancer*, 2004, **4**, 437.
16 N. K. Tafreshi, N. K. Tafreshi, M. C. Lloyd, M. C. Lloyd, J. B. Proemsey, J. B. Proemsey, M. M. Bui, M. M. Bui, J. Kim, J. Kim, R. J. Gillies, R. J. Gillies, D. L. Morse and D. L. Morse, *Mol. Imaging Biol.*, 2016, **18**, 219.
17 K. Okuda, Y. Okabe, T. Kadonosono, T. Ueno, B. G. M. Youssif, S. Kizaka-Kondoh and H. Nagasawa, *Bioconjugate Chem.*, 2012, **23**, 324.
18 X. Han, R. Wang, X. Song, F. Yu, C. Lv and L. Chen, *Biomaterials*, 2018, **156**, 134.
19 R. Weissleder and M. J. Pittet, *Nature*, 2008, **452**, 580.
20 A. Razgulin, N. Ma and J. Rao, *Chem. Soc. Rev.*, 2011, **40**, 4186.
21 L. You, D. Zha and E. V. Anslyn, *Chem. Rev.*, 2015, **115**, 7840.
22 M. H. Lee, J. S. Kim and J. L. Sessler, *Chem. Soc. Rev.*, 2015, **44**, 4185.
23 P. Talukder, S. X. Chen, B. Roy, P. Yakovchuk, M. M. Spiering, M. P. Alam, M. M. Madathil, C. Bhattacharya, S. J. Benkovic and S. M. Hecht, *Biochemistry*, 2015, **54**, 7457.
24 J. L. Yin, L. Huang, L. L. Wu, J. F. Li, T. D. James and W. Y. Lin, *Chem. Soc. Rev.*, 2021, **50**, 12098.
25 R. A. Gatenby, E. T. Gawlinski, A. F. Gmitro, B. Kaylor and R. J. Gillies, *Cancer Res.*, 2006, **66**, 5216.
26 Q. Shi, X. D. Le, B. L. Wang, J. L. Abbruzzese, Q. H. Xiong, Y. J. He and K. P. Xie, *Oncogene*, 2001, **20**, 3751.
27 S. Toyokuni, K. Okamoto, J. Yodoi and H. Hiai, *FEBS Lett.*, 1995, **358**, 1.
28 E. Hileman, J. Liu, M. Albitar, M. Keating and P. Huang, *Cancer Chemother. Pharmacol.*, 2004, **53**, 209.
29 L. Behrend, G. Henderson and R. M. Zwacka, *Biochem. Soc. Trans.*, 2003, **31**, 1441.
30 M. J. Farquharson, A. Al-Ebraheem, G. Falkenberg, R. Leek, A. L. Harris and D. A. Bradley, *Phys. Med. Biol.*, 2008, **53**, 3023.
31 X. Han, R. Wang, X. Song, F. Yu, C. Lv and L. Chen, *Biomaterials*, 2018, **156**, 134.
32 Y. Yue, F. Huo, F. Cheng, X. Zhu, T. Mafireyi, R. M. Strongin and C. Yin, *Chem. Soc. Rev.*, 2019, **48**, 4155.
33 H. Li, Q. Yao, F. Xu, N. Xu, R. Duan, S. Long, J. Fan, J. Du, J. Wang and X. Peng, *Biomaterials*, 2018, **179**, 1.
34 W. Zhang, J. Liu, P. Li, X. Wang, S. Bi, J. Zhang, W. Zhang, H. Wang and B. Tang, *Biomaterials*, 2019, **225**, 119499.
35 F. Kong, Y. Li, C. Yang, X. Li, J. Wu, X. Liu, X. Gao, K. Xu and B. Tang, *J. Mater. Chem. B*, 2019, **7**, 6822.
36 X. Sha, X. Yang, X. Wei, R. Sun, Y. Xu and J. Ge, *Sens. Actuators, B*, 2020, **307**, 127653.

37 Y. Gao, Y. Lin, T. Liu, H. Chen, X. Yang, C. Tian, L. Du and M. Li, *Anal. Chem.*, 2017, **89**, 12488.
38 K. H. Gebremedhin, Y. Li, Q. Yao, M. Xiao, F. Gao, J. Fan, J. Du, S. Long and X. Peng, *J. Mater. Chem. B*, 2019, **7**, 408.
39 J. Zhang, H. Liu, X. Hu, J. Li, L. Liang, X. Zhang and W. Tan, *Anal. Chem.*, 2015, **87**, 11832.
40 R. Peng, J. Yuan, D. Cheng, T. Ren, F. Jin, R. Yang, L. Yuan and X. Zhang, *Anal. Chem.*, 2019, **24**, 15974.
41 F. Xu, H. Li, Q. Yao, H. Ge, J. Fan, W. Sun, J. Wang and X. Peng, *Chem. Sci.*, 2019, **10**, 10586.
42 X. Kong, L. Di, Y. Fan, Z. Zhou, X. Feng, L. Gai, J. Tian and H. Lu, *Chem. Commun.*, 2019, **55**, 11567.
43 A. Chevalier, Y. Zhang, O. M. Khdour, J. B. Kaye and S. M. Hecht, *J. Am. Chem. Soc.*, 2016, **138**, 12009.
44 Z. Li, X. Li, X. Gao, Y. Zhang, W. Shi and H. Ma, *Anal. Chem.*, 2013, **85**, 3926.
45 Y. Wang, L. Zhang, Y. Huang, X. Wang, L. Zhang and L. Chen, *Sens. Actuators, B*, 2020, **310**, 127755.
46 Y. Kwon, J. Oh, M. T. La, H. Chung, S. J. Lee, S. Chun, S. Lee, B. Jeong and H. Kim, *Bioconjugate Chem.*, 2018, **30**, 90.
47 S. Jiao, Si Yang, X. Meng and C. Wang, *Spectrochim. Acta, Part A*, 2020, **241**, 118637.
48 S. Z. Luo, R. F. Zou, J. C. Wu and M. P. Landry, *ACS Sens.*, 2017, **2**, 1139.
49 Z. Q. Zhang, Q. Feng, M. Yang and Y. L. Tang, *Sens. Actuators, B*, 2020, **318**, 128257.
50 Y. Fang, W. Shi, Y. M. Hu, X. Y. Li and H. M. Ma, *Chem. Commun.*, 2018, **54**, 5454.
51 H. D. Li, D. Kim, Q. C. Yao, H. Y. Ge, J. Chung, J. L. Fan, J. Y. Wang, X. J. Peng and J. Y. Yoon, *Angew. Chem., Int. Ed.*, 2021, **60**, 17268.
52 S. S. Wang, X. J. Wu, Y. Q. Zhang, D. Zhang, B. Y. Xie, Z. X. Pan, K. F. Ouyang and T. Peng, *Org. Biomol. Chem.*, 2021, **19**, 3469.
53 S. Karan, M. Y. Cho, H. Lee, H. Lee, H. S. Park, M. Sundararajan, J. L. Sessler and K. S. Hong, *J. Med. Chem.*, 2021, **64**, 2971.
54 J. Ouyang, L. H. Sun, Z. Zeng, C. Zeng, F. Zeng and S. Z. Wu, *Angew. Chem., Int. Ed.*, 2020, **59**, 10111.
55 Y. X. Zou, M. S. Li, Y. L. Xing, T. T. Duan, X. J. Zhou and F. B. Yu, *ACS Sens.*, 2020, **5**, 242.
56 A. W. DeMartino, D. F. Zigler, J. M. Fukuto and P. C. Ford, *Chem. Soc. Rev.*, 2017, **46**, 21.
57 J. Domergue, D. Lison and V. Haufroid, *Int. Arch. Occup. Environ. Health*, 2016, **89**, 835.
58 S. Y. Mo, X. T. Zhang, S. Hameed, Y. M. Zhou and Z. F. Dai, *Theranostics*, 2020, **10**, 2130.
59 L. Fan, Q. Zan, X. D. Wang, S. H. Wang, Y. W. Zhang and C. Dong, *Chin. J. Chem.*, 2021, **39**, 1303.
60 X. W. Li, N. Gao, C. Y. Liu, Y. Zhang, M. J. Su, X. Wang and B. C. Zhu, *Sens. Actuators, B*, 2022, **353**, 131051.
61 H. Zhu, J. L. Fan, J. Y. Wang, H. Y. Mu and X. J. Peng, *J. Am. Chem. Soc.*, 2014, **136**, 12820.
62 X. B. Wang, H. J. Li, Q. B. Li, Y. F. Ding, C. X. Hu and Y. C. Wu, *J. Hazard. Mater.*, 2022, **427**, 127874.
63 Y. J. Yang, M. C. Dai, Y. J. Reo, C. W. Song, S. Sarkar and K. H. Ahn, *Anal. Chem.*, 2021, **93**, 7523.
64 P. P. Lu, C. Y. Zhang, L. L. Fu, Y. H. Wei, Y. Huang, X. Y. Wang and L. X. Chen, *Anal. Chem.*, 2021, **93**, 10378.
65 F. Fan, L. Zhang, X. G. Zhou, F. Y. Mu and G. Y. Shi, *J. Mater. Chem. B*, 2021, **9**, 170.
66 T. Cao, L. Zhang, L. Zheng, J. Qian, A. Iqbal, K. Iqbal, W. W. Qin and Y. Liu, *J. Mater. Chem. B*, 2021, **9**, 4546.
67 T. Zhang, F. J. Huo, W. J. Zhang and C. X. Yin, *Sens. Actuators, B*, 2021, **345**, 130393.
68 H. Xiong, P. Kos, Y. F. Yan, K. J. Zhou, J. B. Miller, S. Elkassih and D. J. Siegwart, *Bioconjugate Chem.*, 2016, **27**, 1737.
69 X. W. Tian, Z. Li, Y. Sun, P. Wang and H. M. Ma, *Anal. Chem.*, 2018, **90**, 13759.
70 M. Li, H. Li, Q. Wu, Y. Li, D. Wang and B. Z. Tang, *iScience*, 2021, **24**, 102261.
71 Y. Chen, X. Zhang, X. Y. Lu, H. W. Wu, D. S. Zhang, B. C. Zhu and S. Y. Huang, *Spectrochim. Acta, Part A*, 2022, **268**, 1386.
72 X. H. Pan, Y. H. Zhao, T. T. Cheng, A. H. Zheng and B. Tang, *Chem. Sci.*, 2019, **10**, 8179.
73 Z. P. She, W. X. Wang, W. L. Jiang, Z. Q. Wang, G. J. Mao and C. Y. Li, *Anal. Chem.*, 2021, **34**, 11826.
74 Y. Zhang, X. F. Zhang, Q. Chen, X. Q. Cao and S. L. Shen, *Sens. Actuators, B*, 2022, **353**, 131145.

